4-2023

Computational fluid dynamics model of hyperthermic intraperitoneal chemotherapy.

Olivia Cooney
University of Louisville

COMPUTATIONAL FLUID DYNAMICS MODEL OF HYPERTHERMIC INTRAPERITONEAL CHEMOTHERAPY

By

Olivia Susan Cooney
B.S. Bioengineering, University of Louisville, 2021

A Thesis
Submitted to the Faculty of the
University of Louisville
J.B. Speed School of Engineering
As Partial Fulfillment of the Requirements
For the Professional Degree

MASTER OF ENGINEERING

Department of Bioengineering

May 2023

COMPUTATIONAL FLUID DYNAMICS OF HYPERTHERMIC INTRAPERITONEAL CHEMOTHERAPY

Submitted by: Olivia S. Cooney Digitally signed by Olivia S. Cooney Date: 2023.04.18 13:41:17 -04'00'

Olivia Cooney

A Thesis Approved on

4/18/2023

By the Following Reading and Examination Committee:

Hermann Frieboes Digitally signed by Hermann Frieboes Date: 2023.04.18 14:49:08 -04'00'

Dr. Hermann Frieboes, Thesis Director

Thomas J. Roussel, Jr. Digitally signed by Thomas J. Roussel, Jr. Date: 2023.04.18 13:17:54 -04'00'

Dr. Thomas Roussel, Committee Member

Nihat Altiparmak Digitally signed by Nihat Altiparmak Date: 2023.04.18 22:36:00 -04'00'

Dr. Nihat Altiparmak, Committee Member

ACKNOWLEDGEMENTS

I would like to thank my Thesis Chair, Dr. Hermann Frieboes, for his constant support and guidance throughout my pursuance of my Master's degree. I would also like to thank Dr. Mouw for his clinical experience and aide in the development of this project. Thank you to Dylan Goodin of Dr. Frieboes' Lab, who stepped in to assist in problem solving and pushed me to dig deeper and constantly learn more. Lastly, I would like to show my deepest gratitude to my family and Alex Revell for their unwavering support throughout my graduate career. They were always there to brighten my days and push me to reach new heights.

ABSTRACT

COMPUTATIONAL FLUID DYNAMICS OF HYPERTHERMIC INTRAPERITONEAL CHEMOTHERAPY

Olivia Cooney

April 18, 2023

Hyperthermic intraperitoneal chemotherapy (HIPEC) is a procedure that targets abdominal tumors in the intraperitoneal space. During the procedure, chemotherapy heated to 40-43^{o}C is cycled through the abdomen for 1 to 2 hours. Although a majority of studies have focused on clinical outcomes, the dynamics of the intra-abdominal flow remain poorly understood. Consequently, it has been difficult to gauge the tumor targeting efficacy, which depends critically on temperature and chemotherapy flow rates. This study establishes a computational framework to evaluate the dynamics of fluid flow during HIPEC, with the goal to enable optimization of tumor drug exposure. A computer aided design (CAD) model of the intraperitoneal cavity was created using SOLIDWORKS coupled with computational fluid dynamics analysis through Ansys Fluent. Probes to measure temperature and flow were placed in the simulated abdomen at seven

areas of interest: under the root of the mesentery, deep pelvis, behind the stomach, behind and under the liver, and between the colon and small bowel. Flow was simulated through catheters placed in forward (superior inlet) and reverse (inferior inlet) directions. Baseline 800cc/min and a 40% increase in flow (1120cc/min) were evaluated under these conditions. The results highlight the potential heterogeneity in temperatures and flow at the various locations of interest as a function of chemotherapy flow rate and direction. The outcome of this study showed that the reverse flow direction (inferior inlets) was optimal compared to forward flow direction (superior inlets) based on temperature distribution over time at the desired probe locations, and should be used in HIPEC treatments going forward, along with an increased flow rate, 1120cc/min. This work represents a first step to in determining optimal input flow rate and flow direction to achieve efficacious tumor targeting during the HIPEC treatment.

TABLE OF CONTENTS

NOMENCLATURE

CAD	Computer aided design
CRS	Cyto-reductive surgery
HIPEC	Hyperthermic intraperitoneal chemotherapy
TCM	Transverse colon mesentery

LIST OF TABLES

LIST OF FIGURES

I. INTRODUCTION

Cancer can invade many different parts of the human body and travel through the blood stream and other tissues. The specific area of concern in this research is the peritoneal cavity. The peritoneal cavity is the space in the abdomen that contains the stomach, small and large intestines, the liver, and the stomach. Peritoneal carcinomatosis is a pathophysiological condition that can metastasize and spread cancer to the peritoneal lining of the abdomen as well as to other surfaces in the peritoneal cavity such as organs through the lymphatics, blood, peritoneal cavity, or direct invasion [1]. There are two main origins of peritoneal carcinomatosis. The first is directly from the peritoneal lining itself, and the second is from other primary organs such as the gastrointestinal tract [1]. Several gastrointestinal and gynecological malignancies have the possibility to grow in the peritoneal cavity [2]. Some organs that can be affected are the stomach, liver, small bowel and mesentery, and transverse colon and mesentery. Peritoneal carcinomatosis significantly decreases the overall survival of patients with liver and/or extraperitoneal metastases from gastrointestinal cancer [2].

The age-adjusted incidence rate of primary peritoneal cancer is 6.78 million [3, 4]. The rate is lowest with black people and highest with white people. The serous membrane lining the abdominal cavity is the peritoneum which supports the abdominal viscera and provides a conduit for blood, lymph, and nerve conduction [4]. There are two layers, the parietal and visceral peritoneum. The parietal peritoneum is attached with the

abdominal wall while the visceral peritoneum surrounds the organs [4]. The abdominal cavity is the space between the two layers. The peritoneum can adapt according to different pathologies and is the largest dynamic membrane that has this ability [4]. The mesodermal layer binds tumor cells with the peritoneum [4]. The 'seed and soil theory' by Stephen Paget describes the carcinogenesis of peritoneal cancers and describes how a malignant tumor gives up cells (seeds) which travel in all directions but only survive and multiply at tumor accepting localizations (soil) [4-6].

One symptom of peritoneal carcinomatosis can be a bowel obstruction due to tumors growing on the small bowel. Symptomatic medications such as antiemetic agents, analgesics, and antisecretory agents can be administered to alleviate this symptom [7]. Bowel obstructions can cause vomiting, abdominal pain, abdominal distension, and anorexia [7].

Diagnosis of peritoneal carcinomatosis can be done using different techniques such as imaging in ultrasounds, CAT scans, NMR scans, and PET/CT positron emission topographies with fluorodeoxyglucose [8]. Treatment is usually needed to resect the obstruction for normal function to return to the peritoneal cavity.

Hyperthermic intraperitoneal chemotherapy (HIPEC) is a treatment indicated for peritoneal carcinomatosis. While HIPEC is only offered at select hospitals, it is estimated that up to 40,000 patients are annually considered eligible for CRS plus HIPEC in the U.S.[9]. In particular, HIPEC is considered for managing digestive tract [10] as well as ovarian [11] cancers. Advantages of the treatment are that a high dose of drug can be administered locally to potentially reach tumors disseminated within the abdominal cavity that may be hard to reach via systemic vasculature while limiting systemic

toxicity. Before the procedure can be performed, cytoreductive surgery (CRS) in which all visible tumors are surgically debulked is performed. This may include the removal of abdominal organs such as the spleen, omentum, and segments of the intestines. A heated chemotherapy solution is then circulated through the abdomen for a period of time, typically 1-2 hours, to treat any residual tumor tissue. The chemotherapy can be applied directly while the abdomen is surgically opened after the CRS [12] or via catheters following abdominal closure [13]. The open technique suffers from heat dissipation, which may reduce its efficacy, while the closed technique may lead to uneven intraperitoneal distribution of solution, potentially yielding excessively high or low local drug concentrations or significant temperature heterogeneity. Closed HIPEC involves filling the abdominal cavity with a solution heated to 42 ^{o}C (107.6 ^{o}F) containing chemotherapy drugs such as mitomycin C or cisplatin, which is then cycled through the abdomen using inflow and outflow catheters in series with a pump. A typical initial volume of fluid would be 4L which is then cycled at 800 cc/min. The benefit of performing HIPEC over other chemotherapy treatments is that it provides localized treatment to the peritoneal cavity over full body chemotherapy treatment.

It is critical for the success of the procedure that the peritoneal surfaces be exposed equally during the duration of therapy while avoiding healthy tissue over-exposure or high temperatures, greater than 43°C [14, 15]. To date, majority studies on HIPEC are concerned with clinical outcomes. Studies have been performed to establish concepts such as the synergism between chemotherapy and hyperthermia [16] and degree of tissue penetration[17]. As such, relatively little is understood about the fluid environment during the procedure. Additionally, there is no clear consensus on how

HIPEC should be performed. An analysis involving a computational fluid dynamic simulation offers a means to evaluate the effect of therapy parameters on potential outcomes.

This study implements a computational fluid dynamics (CFD) model to simulate the flow of solution within the abdominal cavity during closed HIPEC, with the longer-term objective to enable evaluation of different delivery options which may optimize drug exposure and timing for the procedure. The goal is to provide insight into the procedure and offer a means to quantitatively assess its efficiency and efficacy. CFD has been extensively applied in other research studies to study flow in organs and physiological systems, including cardiovascular function [18], aortic [19] and brain aneurysms [20], stomach food digestion [21], hepatic microcirculation [22], lung airflow and aerosol deposition [23], and maternal-fetal umbilical cord heat and blood exchange [24].

II. RELATED LITERATURE

A study was completed at the University of Amsterdam to simulate drug penetration during HIPEC. HIPEC efficacy depends on which chemotherapy treatment used, the concentration of chemotherapy, the carrier solution used, volume of perfusate, perfusate temperature, time duration, patient, and technique of procedure used [17, 25]. Following a successful CRS procedure, patients have a high survival rate than patients who receive an unsuccessful complete CRS procedure [17, 26]. The first three-dimensional CFD model was developed in this study to model drug penetration of a singular tumor nodule embedded in healthy tissue located in the intestine within the peritoneal cavity [17]. Both diffusive forces and convective forces were modeled in the peritoneal cavity. The chemotherapy treatment modeled was cisplatin as it is widely investigated in HIPEC research [17]. Based on Reynolds number calculations, the flow profile was assumed to be laminar as the Reynolds number was only 200. It was found that lower flow velocities delivered less cisplatin to the tumor surface and higher velocities had low flow patterns on the tumor surface and was non-uniform [17]. The study found that larger nodules are more difficult to treat and the most important factors to control drug delivery are velocity and temperature; with velocity, moderate flow between 0.01 and 1m/s are optimal for cisplatin delivery [17]. This simulation study was referenced to determine efficacy of mesh refinement analysis and to provide additional information on drug penetration on tumor nodules during HIPEC.

A retrospective study in Guangzhou, China was conducted to study the safety and effectiveness of high-precision HIPEC in patients. A total of 1,2000 patients were included in the retrospective study. The study used a HIPEC device they developed called "BR-TRG-I-type hyperthermic intraperitoneal perfusion chemotherapy device" (BR-TRG-II; Guangzhou, China). This research aimed to study the safety and effectiveness of HIPEC in general in peritoneal carcinomatosis patients and provide novel methodology in treating peritoneal carcinomatosis[27]. HIPEC is typically delivered for 3 sessions at a perfusion velocity of 450 to 600 cc/min, with inflow temperature of 43°C, and with each session lasting 90 minutes[27]. Patients in this study attempted to receive three sessions of a closed HIPEC post CRS surgery [27] with two inlet and two outlet catheters in "Y" shape with inlet catheters in superior position. The chemotherapy drug and dosage was selected based on the primary tumor and the patient's body weight [27]. Parameters for HIPEC were perfusion set to 90 minutes, perfusion velocity between 450 and 600 mL/min, and inflow temperature set to 43°C. Outflow temperature at time 90 minutes was recorded to be 42±0.2°C [27]. The outcome of this study showed that HIPEC proved safe to treat peritoneal carcinomatosis with low adverse event rates [27]. Results from the retrospective study will be used as validation for the research conducted in this study.

III. METHODS

A. Overview

The model was designed in SOLIDWORKS (V.2021, Dassault Systemes, Waltham, MA), a 3D computer-aided design (CAD) software. The organs modeled were the stomach, liver, transverse colon, transverse colon mesentery, small bowel, and the small bowel mesentery. Other organs and tissue were not modeled, as they are either removed during surgery or do not occupy the intraperitoneal space. Ansys Fluent (Version 2022 R1, Ansys, Inc. Canonsburg, PA), was used to complete the CFD simulation within the modeled anatomy. The study referenced previous research regarding a 3D CFD model of interstitial fluid pressure and drug distribution in heterogeneous tumor nodules during intraperitoneal chemotherapy [28] as well as a 3D CFD simulation modeling drug penetration to tumor nodules in HIPEC [17]. The model is a simplified version of the peritoneal cavity and organs to serve as proof of concept to be detailed in the future using computerized tomography scans (CT-scan).

B. Design of Abdominal Cavity

The developed model implements a 3D cavity shape based on the axial, sagittal, and coronal plane from the standard dimensions for an adult abdomen. A collaborating physician assisted in the modeling of the cavity to assure reasonable approximations of organ proportions. The cavity was created with dimensions 23.12” tall, 9.71” deep, and 15.65” wide. The transverse colon was added so that it would divide the upper third of

the abdomen from the lower portion, and to be attached along the entirety of the posterior abdomen. The diameter of the colon is 2" and total width is 15.52". The stomach was made to attach to the superior aspect of the abdominal cavity and to be locked into place after positioning behind the liver. Between the attachments was open space. The stomach is 7.29" wide, 2.70" deep, and the esophagus diameter is 1.10". The small bowel was modeled first as a 3D trapezoid and then each bowel section was cut out and smoothed to represent a highly simplified version of the small bowel. While the design is simplified, it does occupy 80% of the volume below the transverse colon which is anatomically correct. The length of the small bowel is 9", height of 6" and width of 8". The liver was created to occupy the space in the upper right area of the abdomen. The height is 7.8", 14" from apex to apex, and 7.72" deep. The liver was to be fastened along the edge formed by its upper and posterior surfaces, attaching on the anatomical right side posterior aspect of the abdominal wall. Dimensions of the cavity and organs are summarized in **Table 1**.

C. Design of Final Assembly

The final assembly was created from each part file. The posterior and anterior wall part file was imported into an assembly in SOLIDWORKS as the reference point. A circular extrusion was made on the superior surface of the wall for the esophagus of the stomach. The stomach was mated to the cavity wall through the esophageal attachment point located on the part. The mate was made by making the circles tangent and coincident. Next, the transverse colon and mesentery were mated to the cavity wall. Two circles were extruded from the left and right side of the cavity wall to mate to the colon. The circles were made tangent and coincident to attach the colon to the cavity wall. The

transverse colon was located one-third down from the front of the cavity position. The mesentery of the colon was locked in place after ensuring a connection between the posterior wall and mesentery.

The liver was then imported into the assembly and positioned in the uppermost, superior left hand corner. Once that attachment was made, the liver was placed on top of the stomach and above the transverse colon. A mated lock was used to secure the position of the liver. Lastly, the small bowel and mesentery was inserted into the cavity. The small bowel was located inferior to the transverse colon. The mesentery of the small bowel ran parallel to the transverse colon. No attachment points were made between the small bowel and cavity wall. Both the mesentery and small bowel were free floating in the abdominal cavity. The bowel was mated by locking it in place with the cavity wall. The final cavity assembly can be seen in **Figure 1**. Probes to measure temperature and flow were placed, in Ansys Fluent, in the simulated abdomen at seven areas of interest: under the root of the mesentery, deep pelvis, behind the stomach, behind and under the liver, and between the colon and small bowel. To calculate standard deviations for the temperature and velocity magnitude at each of the probe locations, 3 rake probes were used in each location and can be seen in **Figure 2**.

D. Design and Placement of Catheters

One catheter part was used to model both inflow and outflow types for the simulation. To represent the catheter, 0.4” diameter holes were cut through the cavity with a boss base extrusion that extends 3.00” internally in the cavity. This simplified catheter design was used as the faces inside the peritoneal cavity would be used as the boundary conditions for inflow and outflow of fluid.

Catheters were placed at the superior and inferior portions of the cavity. Two catheters at each portion were inserted to simulate the V-shaped catheter used in clinical practice. The faces inside of the peritoneal cavity were used as the surface to define inlet boundary conditions. Because there were two inlet surfaces, the desired flow rate (either 800cc/min for normal flow or 1120cc/min for increased flow) had to be divided by two and each face was set to the calculated value (each face was set to 0.0133 m/s for regular flow and 0.0187 m/s for the increased flow rate).

E. Numerical Methods

Ansys Fluent was used for the CFD simulation. A pressure-based solver was used for the simulation over a density-based solver as typically, a density-based solver is recommended for high-speed compressible flow and in this simulation, an incompressible flow was modeled [29]. Also, the pressure-based solver solves the pressure equation to conserve mass, which is of interest. The pressure-velocity coupling scheme was chosen as it controls the manner in which pressure and velocity are updated when the pressure-based solver is chosen [30]. Coupling pressure and velocity was chosen due to the robust properties for transient solutions that a coupled solver provides [30].

The pressure-velocity coupling scheme used was the SIMPLEC (SIMPLE-Consistent) algorithm, due to the benefit of the increased under-relaxation that can be applied. Under-relaxation factors increase the stability of the simulation by dampening the solution. Under-Relaxation factors for the solution control were set as follows: pressure = 0.3, density = 1, body forces = 1, momentum = 0.7, turbulent kinetic energy = 0.8, specific dissipation rate = 0.8, turbulent viscosity = 1, and energy = 1. 0 skewness correction and the Rhie-Chow: distance-based flux type were used. As this simulation has

a complicated, turbulent flow, SIMPLEC aides in improving convergence by being limited by the pressure-velocity coupling [30].

The least squares cell based spatial discretization gradient was used. Spatial discretization scheme for pressure was set to second order, and second order upwind was set for momentum, turbulent kinetic energy, specific dissipation rate, and energy. First order implicit scheme for transient formulation discretization was used. Transient simulations were performed to resolve solver preferences at 0.25s time step for 90 minutes.

F. General Equations

In using the pressure-based solver approach, the velocity field is obtained from the momentum equations and the pressure field is extracted by solving a pressure equation by manipulating continuity and momentum equations [30]. The pressure-based solver uses an algorithm, the projection method, wherein the constraint of mass conservation of the velocity field is gained by solving for pressure [30]. Pressure is derived from continuity and momentum equations in that the velocity field, corrected by pressure, satisfies continuity [30]. The governing equations are solved repeatedly until the solution converges due to the equations being nonlinear and coupled [30]. The Navier-Stokes equation governs the fluid dynamic equations and can be described by the momentum and mass conservation equations. The conservation of mass equation can be written as (Eq.1)[30],

$$\frac{\partial \rho}{\partial t} + \nabla \cdot (\rho \vec{v}) = S_m \quad (1)$$

where ρ is the density, $\vec{v}$ is the velocity vector and the source, S_m , is the mass added to the continuous phase from dispersed second phase [30].

The conservation of momentum is described by (Eq. 2)[30],

$$\frac{\partial}{\partial t}(\rho\vec{v}) + \nabla \cdot (\rho\vec{v}\vec{v}) = -\nabla \mathrm{p} + \rho + \rho\vec{g} + \vec{F}\,, \tag{2}$$

where ρ is the density, $\vec{v}$ is velocity vector, p is static pressure, $\rho\vec{g}$ is gravitational body force, and $\vec{F}$ is external body forces.

G. Flow Profile

To determine turbulent or laminar fluid flow, the Reynolds number was calculated using,

$$Re = \frac{V \cdot L}{\upsilon} = \frac{\frac{Q}{A} \cdot L}{\left(\frac{\mu}{\rho}\right)} = \frac{Q\rho L}{\mu A} \tag{3}$$

where V is the flow velocity [m/s], computed from the average fluid flow rate (m^3/s) and area (m) of the catheter (*Q* and *A*, respectively). L is the characteristic length [m], and the kinematic viscosity, *v*, of the fluid [m^2/s] is represented using the dynamic viscosity, μ (kg/m-s) and the density (kg/m^3). Using the maximum fluid flow rate of 1120 cc/min (1.8667×10^{-5} m^3/s), the density of water (991.47 kg/m^3), diameter of catheter (0.01016m), dynamic viscosity of 6.302×10^{-4} kg/m-s and area of catheter as 3.24293×10^{-4} m^2, we find

$$Re_{max} = \frac{\left(1.8667x10^{-5}\frac{m^3}{s}\right)\left(991.47\frac{kg}{m^3}\right)(0.01016m)}{\left(6.302x10^{-4}\frac{kg}{ms}\right)(3.24293x10^{-4}m^2)} \approx 3{,}759. \tag{4}$$

Turbulency depends on the geometry of the fluid flow region. In fully developed pipe flow, this transition occurs around Re = 2300 [17]. Therefore, the Reynolds number in this simulation determines turbulency. The k-omega SST turbulency model was used in the simulation.

H. Grid Independence

Grid independence in this simulation was ensured through mesh refinement (**Figure 3A**). Mesh sensitivity analysis was performed with three levels of resolution: low, medium, and high resolution meshes. The low-resolution mesh contained 158859 nodes and 803073 elements. The medium-resolution mesh contained 212444 nodes and 1069090 elements. Lastly, the high-resolution mesh contained 786837 nodes and 4081208 elements. The temperature at the outlet was the parameter used to compare the mesh refinements. The outlet temperature for each mesh size were similar with percent error between low and medium mesh of 0.0332, medium and high of 0.0055, and high and low of 0.0387. Since the percent error between the medium and high mesh was not statistically significant, the results of this study can be regarded as grid independent, and the medium refined mesh should be used to calculate results in the remainder of the study.

I. Time Step Independence

Time step independence was determined through time step sensitivity analysis for both the outlet temperature (**Figure 3B**) and the temperature for each probe location at 5400s (**Figure 3C**). Time step sizes analyzed were 0.0625s, 0.25s, and 1s. Outlet temperature was the parameter chosen to compare between time step sizes for the first

analysis. In this analysis, the percent error between 0.0625s and 0.25s was 0.00071, 0.25s and 1s was 2.93×10^{-5}, and 1s and 0.0625s was 0.00073. In the second analysis, outlet temperature was chosen as the parameter to be evaluated for each probe location. Based on the data shown in **Figure 3B and 3C**, the model is time step independent and 0.25s was chosen for simulations moving forward.

J. Simulation Parameters and Initial Conditions

To further define the study, the following steps were taken to set up the initial conditions and definitions of the simulation. The time dependent variables were set to run for 5400s. The fluid in the model was set to water and the solids were set to user defined materials for the tissue models defined later in the setup. The material properties of water were used to simulate chemotherapy drugs as cisplatin, a common chemotherapy drug administered during HIPEC, is diluted in a water based medium. Material properties of the chemotherapy drug vs. material properties of water would have negligible effects on fluid dynamics. The initial fluid conditions were set to a temperature of 316.15 K (42°C). User defined materials were assigned to each organ using values gathered from a tissue property database provided by the IT'IS Foundation [31], as listed in **Table 2**. The density, thermal conductivity, and heat capacity of each tissue type were thus defined within the software. Each tissue model was then able to be set to its respective material. The material properties for water used in the model are as follows: density of 998.2 kg/m^3, specific heat of 4182 J/(kg K), thermal conductivity of 0.6 W/(m K), and viscosity of 0.001003 kg/(m s). Catheters were given material properties of silicone rubber with a density of 1400 kg/m^3, specific heat of 1175 J/(kg K), and thermal conductivity of 0.6 W/(m K). The cavity itself was modeled as an enclosure in ANSYS Design Modeler and

thus was set as fluid cell zone conditioning for the simulation. Cell zone conditions for the liver, small bowel and mesentery, liver, and transverse colon were set to solid. Lastly, boundary conditions were set to define the inlet and outlet conditions. For the baseline study, the inlets were set in the superior position (forward flow) and outlets in the inferior position. The inlet boundary condition was set to a mass-flow inlet with baseline flow rate, provided by the collaborating surgeon, of 0.0133 kg/s (800cc/min) and an initial gauge pressure of 0 Pa, as well as a 5% turbulent intensity and turbulent viscosity ratio of 10. Inlet temperature was set to 316.15K (42°C). Outlet boundary condition was set to pressure outlet with a gauge pressure of 0 Pa, backflow pressure specification of total pressure, 5% backflow turbulent intensity and a backflow turbulent viscosity ratio of 10 which are the default values in Ansys Fluent. Outlet temperature and outlet flow rate were set as convergence criterion.

After the baseline condition of 800cc/min, forward flow was completed, three subsequent simulations were run. The first simulation was in the reverse direction (inlets in superior position) with flow rate set to 800cc/min (0.0133 kg/s) with all the same material properties and boundary conditions as in the first trial. Second, a simulation was run with a 40% increase of flowrate of 1120cc/min (0.01867 kg/s) in the forward position (superior inlets). Lastly, a reverse flow (inferior inlets) simulation was run with increased flow rate of 1120cc/min (0.01867 kg/s).

III. RESULTS

A. Simulation Results

The simulated abdominal cavity structure is shown in **Figure 1**. Catheters were placed at the superior and inferior portions of the cavity as shown (**Figure 1C**). Two catheters on each end were inserted to simulate the V-shaped catheter used in clinical practice. Probes were placed at points of interest within the cavity (**Figure 2**), with locations as defined in **Table 3**. Flow rate values were expressed as velocity magnitudes as amount of flow, not direction, was of interest.

A forward flow of 800 cc/min from the superior to the inferior parts of the cavity represents the standard clinical setting. A 40% increase in this flow (1120 cc/min) was also evaluated, as well as reverse flow from the inferior to the superior position. The average change in fluid temperature with respect to time within the cavity for each of these conditions is shown in **Figure 4**. Data was retrieved every 600s.

Figure 4A shows the average change in fluid temperature at each probe location with respect to time of forward flow of 800cc/min. This graph shows that average change of temperature is ~0.004 K/s at t=600s of the simulation vs. the end (t=5400s). Probe 2, located inferior to the small bowel mesentery, is the only exception where the average change in temperature begins at 0 at t=600s and finishes the simulation at 0.001038 K/s. With this probe being located so closely to the small bowel mesentery, the temperature not stabilizing in this location is not surprising. The mesentery creates a challenge for

flow profile as it is difficult for fluid to reach the areas between each “level” of bowel. This would explain why at t=5400, the change in temperature is slightly greater than the other probes and does not converge to 0 with a decreased flow rate.

Figure 4B shows the average change in fluid temperature at each probe location with respect to time of forward flow of 1120cc/min. Again, probe 2 (inferior to small bowel mesentery) started at 0 K/s and ended at 0.000610 K/s. The standard deviations (n=3) were higher at the beginning of the simulation and gradually lessened over the course of the simulation. Toward the end of the simulation, probe 7 (posterior to liver) started a cyclical pattern of increasing and decreasing in change of temperature. Probes 4, 5, and 7 all ended with negative change in temperature over time which indicates that these locations are losing temperature to the fluid.

Figure 4C shows the average change in fluid temperature at each probe location with respect to time of reverse flow of 800cc/min. With a reverse flow, the change in temperature with respect to time is increased at the beginning and converges to 0 at the end of the simulation (t=5400s). Again, the standard deviations at the end of the simulation are relatively 0. This graph shows that as the simulation progresses, the change in temperature decreases, meaning that the chemotherapy drugs are not losing temperature to the organs.

Figure 4D shows the average change in fluid temperature at each probe location with respect to time of reverse flow of 1120cc/min. This graph mimics **Figure 4C**, however in this dataset, probe 2 (inferior to small bowel mesentery) starts out high in the beginning of the simulation and converges to 0 at the end of the simulation. With the

increased flow rate, the fluid was able to reach the mesentery locations and allowed for the fluid to interact with organ.

Flow rates and fluid temperatures recorded by each probe location in time for 800cc/min forward and reverse flow as well as 1120cc/min forward and reverse flow are shown in **Figure 5**. During forward flow, probe 2 (inferior to small bowel mesentery) has low temperatures compared to the other probe locations (**Figure 5A** and **Figure 5B**). Again, this is due to the challenges that the small bowel poses for fluid to reach target tissue in this area as well as the probe location being below the TCM which receives a lower flow and thus, not reaching as high of temperatures as above the TCM. In the reverse flow direction, the probe 2 temperature was able to reach ~312K at t=5400s (**Figure 5C** and **Figure 5D**) due to the proximity to the inlet (inferior position). Based on these data sets, the reverse flow results in a steady increase of temperature representing moderate hyperthermia which is considered successful in HIPEC.

Figure 6 depicts the velocity magnitude (m/s) over time at t=600s and t=5400s. In the forward direction (**Figure 6A** and **Figure 6B**), the increased velocity magnitudes at probe 2 (inferior to small bowel mesentery) and probe 6 (posterior to stomach). This is due to vertexing occurring at these locations. In the reverse flow direction (**Figure 6C** and **Figure 6D**), the velocity magnitude is lower than the forward flow direction. Reversing the flow with inlet at the inferior position of the abdomen shows decreased velocity magnitude in probes 3, 4, 5, 6 and 7 due to the barrier to flow created by the TCM (**Figure 6C and Figure 6D**).

The differences in fluid temperatures and in flow rates comparing forward vs. reverse inlet flow as well as 800 vs. 1120cc/min flow rates are quantified by time 5400s

at each probe location in **Figure 7**, highlighting the potential heterogeneity between the various probe locations. In **Figure 7A**, the difference in temperature between forward and reverse flows was high at probes 2 and 3 for both flow rates, and high for probe 4 at 800cc/min. In **Figure 7B**, the difference in velocity magnitude between forward and reverse directions of the fluid was low at all probe locations. **Figure 7C** shows that the difference in temperature between 800cc/min and 1120 cc/min is higher at probe 2 for both directions. **Figure 7D** shows the difference in velocity magnitude is increased at probe location 2 for both flow directions, and probes 4, 5, 6 for the reverse flow. Overall, the results indicate that flow rate does not influence the difference in temperature in relation to inlet direction (forward vs. reverse) but does influence flow velocity magnitude in both directions at probe 2 and an increased effect in the reverse direction at probes 3, 4, 5, 6, and 7. The results also indicate that the flow direction has an effect on the temperature for both 800cc/min and 1120cc/min at probes 3 and 4 but does not influence flow velocity magnitude for either flow rate.

B. Validation

A real-world, retrospective study, completed in Guangzhou, China, titled "Safety and Effectiveness of High-Precision Hyperthermic Intraperitoneal Perfusion Chemotherapy in Peritoneal Carcinomatosis: A Real-World Study" is used to validate this study. In this study, there was a total patient population of 1,200. Typically, 3 sessions of HIPEC were performed at flow rates of 450 to 600 cc/min, with inflow temperature of 43°C, and with each session lasting 90 minutes[27]. The two inlet and two outlet catheters were inserted in V-shape with inlet catheters in superior position. The chemotherapy drug and dosage was selected based on the primary tumor and the patient's

body weight [27]. Outlet temperatures at 0 min, 30 min, 60 min, 90 min, and 120 min were recorded in this study. At time t=0 min, the outflow temperature was recorded to be 39.6±0.7°C [27]. At t=30 min, outflow temperature was 41.9±0.2°C, while at t=60 min, outflow temperature was recorded as 42.0±0.2°C [27]. At time t=90 min, outflow temperature was 42.0±0.1°C and ended the simulation at t=120 min with an outflow temperature of 39.7±0.2°C [27].

In the CFD model, using forward direction flow (superior inlets) and 800cc/min flow rate for 90 minutes, the outlet temperature was recorded to be 311.53K (38.38°C). The percent error between the CFD simulation and the real-world study for outlet temperature is 8.26%.

IV. DISCUSSION

This study implements a computational fluid dynamic simulation of the abdominal cavity and associated key organs to evaluate the effect of therapy parameters on potential outcomes of the HIPEC procedure. Two flow rates and two inlet positions were evaluated to determine best practices for HIPEC success The simulations enable evaluation of flow rate, inlet flow direction, and fluid temperature within the cavity. This data provides a comprehensive evaluation of how the internal abdominal environment might affect temperatures and flow during HIPEC. It was found that a reasonable temperature equilibrium develops over the course of the procedure and that the procedure is susceptible to variations in technique which may impact clinical efficacy.

CFD simulations have been used in other research studies extensively to study flow in organs and physiological systems. Some examples include cardiovascular function [18], aortic [19] and brain aneurysms [20], stomach food digestion [21], hepatic microcirculation [22], lung airflow and aerosol deposition [23], and maternal-fetal umbilical cord heat and blood exchange [24]. Drug penetration in tumor nodules during HIPEC has also been studied [17]. The outcome of this study determined that the most important factors to control drug delivery are velocity and temperature; with velocity, moderate flow between 0.01 and 1m/s are optimal for cisplatin delivery [17].

Additionally, clinical studies have been performed to evaluate outcomes of HIPEC [27]. Results from this study proved the HIPEC safe to treat peritoneal carcinomatosis with low adverse event rates [27].

In this study, the results highlight the heterogeneity introduced by variation of the procedure parameters. As the simulation progressed, the change in temperature over time converged to 0 K/s (**Figure 4**). By reversing the flow direction, the peritoneal cavity intrabdominal temperature was more homogenous than in the forward direction (**Figure 5**) and were closer to target temperatures of 39-40°C. Velocity magnitudes at each probe location were also lower in the reverse flow rejection than in the forward flow direction (**Figure 6**). **Figure 6** also indicates that in the reverse direction, the flow velocity is greater at 1120cc/min than 800cc/min. There does not seem to be a difference in flow velocity magnitudes from t=600s to t=5400s (**Figure 6**). Results in **Figure 7A** and **Figure 7B** indicate that the flow direction influences the temperature for both 800cc/min and 1120cc/min at probes 3 and 4 but does not influence flow velocity magnitude for either flow rate. Results in **Figure 7C** and **Figure 7D** indicate that flow is homogenous for temperature in relation to inlet direction (forward vs. reverse) but is heterogenous in relation to inlet positioning temperature and flow velocity at probe 2. The flow rate has an increased effect on flow velocity in the reverse direction at probes 3, 4, 5, 6, and 7.

The findings in this simulation represent an important first step in understanding the shortcomings of the HIPEC technique, which with further analysis taking into consideration patient variables could lead to optimization. This model used forward direction flow (superior inlets) and 800cc/min flow rate for 90 minutes. The outlet temperature was recorded to be 311.53K (38.38°C). The percent error between this study

and the real-world, retrospective study, completed in Guangzhou, China [27] for outlet temperature is 2.947%. This difference could be due to the decreased flow rate in the real-world study than in the CFD model. Further validation should be completed with more clinical data at different flow rates and flow directions.

A significant decrease in temperature and flow by 5400s may be partially due to obstruction to the reverse flow caused by the structures in the abdomen. Different catheter inlet locations are expected to yield correspondingly different temperature and flow conditions, which could be evaluated to maintain desired temperatures during the duration of the procedure and to attempt minimizing the heterogeneity in temperature. The combination of different locations and flow rates could thus be dynamically adjusted to optimize outcomes. Further, dynamically varying flow directions could also be evaluated. The results suggest that such changes would be expected to yield significant differences in intraperitoneal heat distribution.

One restriction of this simulation is the organs being modeled as solids and not with viscoelastic properties. It is proposed in future work to mobilize and add mechanical properties to the tissue models. Human tissue is a nonlinear elastic material that also has viscoelastic properties which are difficult to define in CFD modeling. Another limitation of this study is the simplification of the anatomy. In future work, it would be beneficial to use CT scans to create the 3D CAD organs. This study focused on the thermal properties as an essential first step to correctly simulating the procedure. Moving forward, the model could incorporate findings from other CFD research in drug penetration during HIPEC. Doing so would allow for a more realistic approximation of the procedure and aid in the ability to translate these findings to clinical practice. An extensive exploration

of flow parameters was not undertaken in this pilot study. In future studies, lower flow rates, increased inlet temperatures, increased number of probes should be studied to further isolate the proper parameters for efficient and effective HIPEC. However, even the limited number of flow parameters tested in this study demonstrate how variable the quality of HIPEC may be with relatively minor changes in technique. Further work should be completed to further validate these findings in the clinical setting. Temperature distributions in human subjects would provide insight into the variability in flow behavior between individual patients as well as between different techniques or catheter arrangements. After further validation, optimal flow parameters including catheter position and numbers could be established to minimize heterogeneity in drug delivery and temperature. Ideally, the dimensions of the cavity and the organs could be specified to match those of individual patients, allowing for personalization of the treatment.

Considering the observations on flow rate, velocity magnitude, outlet temperature, and temperature distribution in this study, it is suggested that HIPEC should be performed with reverse flow rate (inferior inlet) at a flow rate of 1120cc/min. These surgical parameters are ideal for multiple reasons. The first is that the average change in temperature with respect to time consistently converges to 0 at each location of interest (**Figure 4D**). Second, the temperature distribution across the cavity results in a steady increase of temperature (**Figure 5D**), especially probe location 2 (inferior to small bowel mesentery) which is a major area of concern for temperature distribution and fluid interaction as this area is difficult for fluid to reach due to the TCM, anatomical positioning, and organ design. Lastly, the reverse flow direction at 1120 cc/min had increased velocity magnitude.

With further simulation development, the simulation could be designed to assist in determining patient specific treatment plans for flow rate, inlet position, and inlet temperature parameters. This work represents a first step in determining appropriate input flow rate and inlet catheter positioning to achieve efficacious tumor targeting during the HIPEC procedure.

REFERENCES

1. Pletcher E, G.E., Labow D, *Peritoneal Cancers and Hyperthermic Intraperitoneal Chemotherapy.* Surg Clin North Am, 2020. **100**(3): p. 589-613.
2. Coccolini F, G.F., Lotti M, Virzì S, Iusco D, Ghermandi C, Melotti R, Baiocchi G, Giulini SM, Ansaloni L, Catena F, *Peritoneal carcinomatosis.* World J Gastroenterol, 2013. **19**(41): p. 6979-94.
3. Goodman MT, S.Y., *Incidence of ovarian, peritoneal, and fallopian tube carcinomas in the United States.* Cancer Epidemiol Biomarkers Prev, 2009. **18**(1): p. 132-9.
4. Anwar A, K.A., *Peritoneal Cancer.* StatPearls, 2021.
5. Langley RR, F.I., *The seed and soil hypothesis revisited--the role of tumor-stroma interactions in metastasis to different organs.* Int J Cancer, 2011. **128**(11): p. 2527-35.
6. Mikuła-Pietrasik J, U.P., Tykarski A, Książek K, *The peritoneal "soil" for a cancerous "seed": a comprehensive review of the pathogenesis of intraperitoneal cancer metastases.* Cell Mol Life Sci, 2018. **7**(4): p. 5715-26.
7. Guillemette Laval, B.M.-B., Frédéric Guirimand, Laure Chauvenet, Laure Copel, Aurélie Durand, Eric Francois, Martine Gabolde, Pascale Mariani, Christine Rebischung, Vincent Servois, Eric Terrebonne, Catherine Arvieux,, *Recommendations for Bowel Obstruction With Peritoneal Carcinomatosis.* Journal of Pain and Symptom Management, 2014. **48**(1): p. 75-91.
8. Castro-Mesta, J.F., et al., *Bases and Foundations of the Treatment of Peritoneal Carcinomatosis: Review Article.* Medicina Universitaria, 2016. **18**(71): p. 98-104.
9. Rahul Rajeev, B.K., and Kiran K. Turaga, *Impact of surgical volume of centers on post-operative outcomes from cytoreductive surgery and hyperthermic intra-peritoneal chemoperfusion.* J Gastrointest Oncol, 2016. **7**(1): p. 122-8.
10. Gesson-Paute, A.l.M.D., et al., *Pharmacokinetics of Oxaliplatin During Open Versus Laparoscopically Assisted Heated Intraoperative Intraperitoneal Chemotherapy (HIPEC): An Experimental Study.* Annals of Surgical Oncology, 2008. **15**(1): p. 339-344.
11. Armstrong, D.K., et al., *Intraperitoneal cisplatin and paclitaxel in ovarian cancer.* N Engl J Med, 2006. **354**(1): p. 34-43.
12. Sugarbaker, P.H., W. Yu, and Y. Yonemura, *Gastrectomy, peritonectomy, and perioperative intraperitoneal chemotherapy: the evolution of treatment strategies for advanced gastric cancer.* Semin Surg Oncol, 2003. **21**(4): p. 233-48.
13. Boutros, C., P. Somasundar, and N.J. Espat, *Early results on the use of biomaterials as adjuvant to abdominal wall closure following cytoreduction and hyperthermic intraperitoneal chemotherapy.* World J Surg Oncol, 2010. **8**: p. 72.

14. Neuwirth, M.G., H.R. Alexander, and G.C. Karakousis, *Then and now: cytoreductive surgery with hyperthermic intraperitoneal chemotherapy (HIPEC), a historical perspective.* J Gastrointest Oncol, 2016. **7**(1): p. 18-28.
15. Olivier Glehen, E.C., Shigeki Kusamura, Marcello Deraco, Dario Baratti, Guillaume Passot, Annie-Claude Beaujard, and Gilly Francois Noel, *Hyperthermic Intraperitoneal Chemotherapy: Nomenclature and Modalities of Perfusion.* Journal of Surgical Oncology, 2008. **98**: p. 242-246.
16. Santiago Gonzalez-Moreno, L.A.G.-B., and Gloria Ortega-Perez, *Hyperthermic intraperitoneal chemotherapy: Rationale and technique.* World J Gastrointest Oncol., 2010. **2**(2): p. 68-75.
17. Daan R. Löke, R.F.C.P.A.H., Nicolaas A. P. Franken, Arlene and P.J.T. L. Oei, Johannes Crezee & H. Petra Kok, *Simulating drug penetration during hyperthermic intraperitoneal chemotherapy.* Drug delivery, 2021. **28**(1): p. 145-161.
18. Morris, P.D., et al., *Computational fluid dynamics modelling in cardiovascular medicine.* Heart, 2016. **102**(1): p. 18-28.
19. Soudah, E., et al., *CFD modelling of abdominal aortic aneurysm on hemodynamic loads using a realistic geometry with CT.* Comput Math Methods Med, 2013. **2013**: p. 472564.
20. Sforza, D.M., C.M. Putman, and J.R. Cebral, *Computational fluid dynamics in brain aneurysms.* Int J Numer Method Biomed Eng, 2012. **28**(6-7): p. 801-8.
21. Ferrua, M.J. and R.P. Singh, *Modeling the fluid dynamics in a human stomach to gain insight of food digestion.* J Food Sci, 2010. **75**(7): p. R151-62.
22. Debbaut, C., et al., *Perfusion characteristics of the human hepatic microcirculation based on three-dimensional reconstructions and computational fluid dynamic analysis.* J Biomech Eng, 2012. **134**(1): p. 011003.
23. Nowak, N., P.P. Kakade, and A.V. Annapragada, *Computational fluid dynamics simulation of airflow and aerosol deposition in human lungs.* Ann Biomed Eng, 2003. **31**(4): p. 374-90.
24. Kasiteropoulou, D., A. Topalidou, and S. Downe, *A computational fluid dynamics modelling of maternal-fetal heat exchange and blood flow in the umbilical cord.* PLoS One, 2020. **15**(7): p. e0231997.
25. Helderman, R., et al., *Variation in Clinical Application of Hyperthermic Intraperitoneal Chemotherapy: A Review.* Cancers, 2019. **11**(1): p. 78.
26. Cavaliere, F., et al., *Prognostic factors and oncologic outcome in 146 patients with colorectal peritoneal carcinomatosis treated with cytoreductive surgery combined with hyperthermic intraperitoneal chemotherapy: Italian multicenter study S.I.T.I.L.O.* European Journal of Surgical Oncology (EJSO), 2011. **37**(2): p. 148-154.
27. Mingchen ba, S.C., Hui Long, Yuanfeng Gong, Yinbin Wu, Kunpeng Lin, Yinuo Tu, Bohuo Zhang, and Wanbo Wu, *Safety and Effectiveness of High-Precision Hyperthermic Intraperitoneal Perfusion Chemotherapy in Peritoneal Carcinomatosis: A Real-World Study.* Frontiers in Oncology, 2021. **11**.
28. Steuperaert, M., et al., *A 3D CFD model of the interstitial fluid pressure and drug distribution in heterogeneous tumor nodules during intraperitoneal chemotherapy.* Drug Deliv, 2019. **26**(1): p. 404-415.

29. School, W.S. *Water Compressibility*. 2018 [cited 2023.
30. *Ansys® Academic Research Fluids, Help System, Ansys Fluent User's Guide*. Ansys, Inc.
31. Hasgall, P.A., et al. *IT'IS database for thermal and electromagnetic parameters of biological tissues,*. (Version 4.0) 2018; Available from: www.itis.ethz.ch/database.

APPENDIX

TABLE 1 - DIMENSIONS OF THE ABDOMINAL CAVITY AND THE ORGANS SIMULATED USING ANSYS FLUENT

Component	**Height (in)**	**Depth (in)**	**Width (in)**
Cavity	23.12	9.71	15.65
Transverse Colon	2.75	2.00 (diam)	15.52
Stomach	4.42	2.70	7.29
Esophagus	4.16	2.74	1.10 (diam)
Small Bowel	9.00	6.00	8.00
Liver	7.83	7.72	14.02 (apex to apex)

TABLE 2 - MATERIAL PROPERTIES USED IN SIMULATION.

Tissue Type	**Density (kg/m^3)**	**Heat Capacity ($J/kg/^0C$)**	**Thermal Conductivity ($W/m/^0C$)**
Stomach	1088	3690	0.53
Liver	1079	3540	0.52
Transverse Colon	1088	3655	0.54
Small intestine	1030	3595	0.49
Silicone Rubber	1400	1175	0.60

TABLE 3 - LOCATION OF PROBES WITHIN THE SIMULATED ABDOMINAL CAVITY

Probe #	**Location**
1	Between small and large bowels
2	Inferior to small bowel mesentery
3	Next to duodenum
4	Superior to liver
5	Superior to fundus
6	Posterior to stomach
7	Posterior to liver

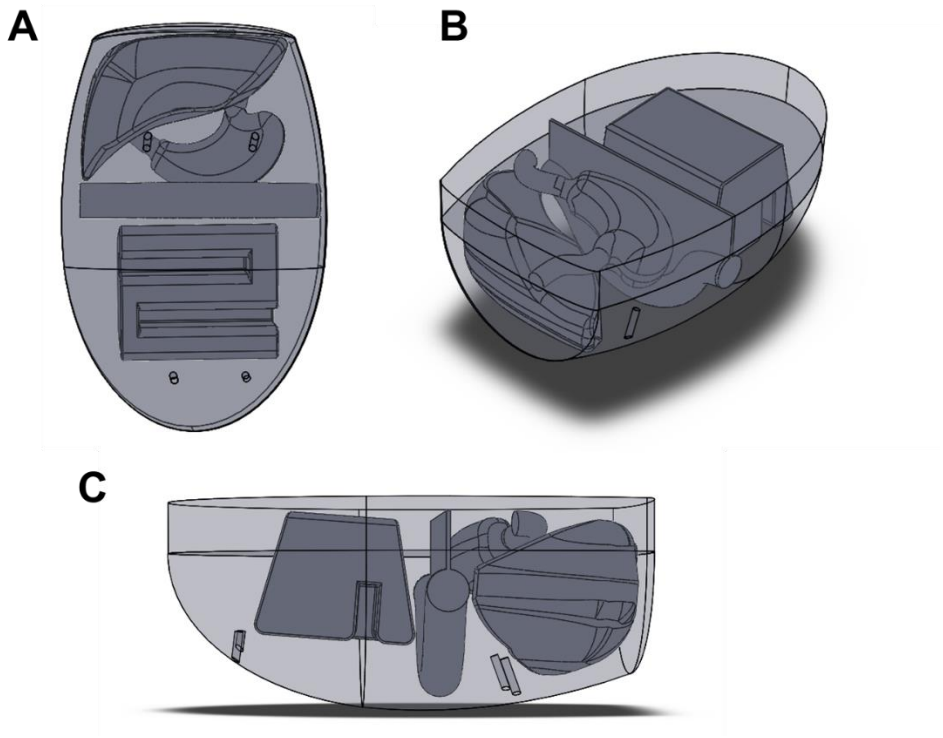

FIGURE 1 - Abdominal cavity simulated in SOLIDWORKS. (A) Anterior view; (B) Isometric view; (C) Positioning of catheters at top and bottom of cavity (dual inlet and outlets were used to represent the V-shaped catheters).

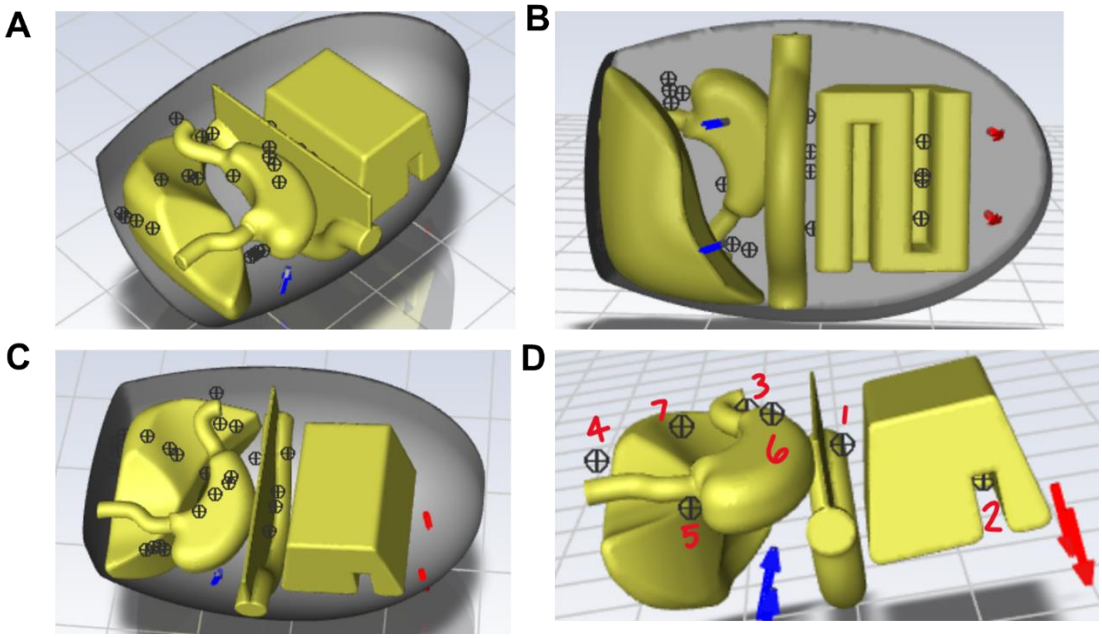

FIGURE 2 - Location of 4 probes in 7 areas of interest within the cavity. (A) Isometric view; (B) Anterior view; (C) View of catheters from posterior view (D) Probe locations numbered. NOTE: 4 probes were placed at each of the 7 areas of interest.

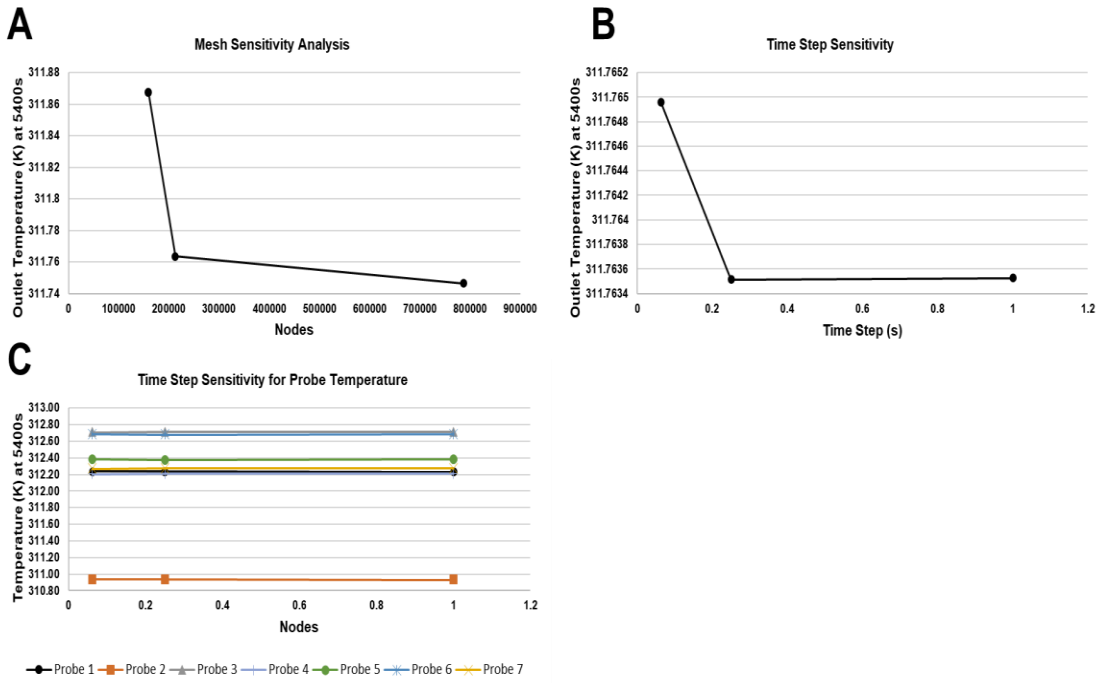

FIGURE 3 - Sensitivity Analyses. (A) Mesh sensitivity analysis with low, medium, and high resolution meshes. (B) Time step sensitivity analysis with time steps sizes of 0.0625s, 0.25s, and 1s. (C) Time step analysis for each probe location at time step sizes of 0.0625s, 0.25s, and 1s.

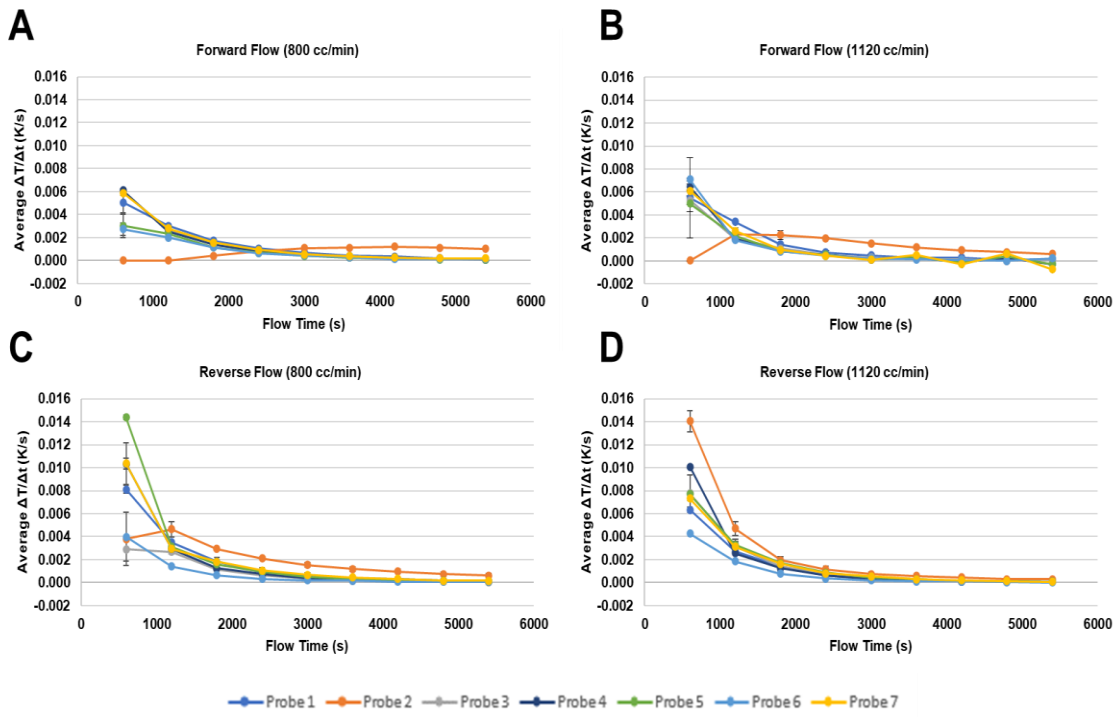

FIGURE 4 - Average change in temperature (T) with respect to time (*t*) within the cavity at each probe location. (A) Forward flow (superior inlet) at baseline 800 cc/min; (B) Forward flow (superior inlet) at 1120cc/min representing a 40% increase from baseline; (C) Reverse flow (inferior inlet) at 800cc/min; (D) Reverse flow (inferior inlet) at 1120 cc/min. Error bars: SD n=3

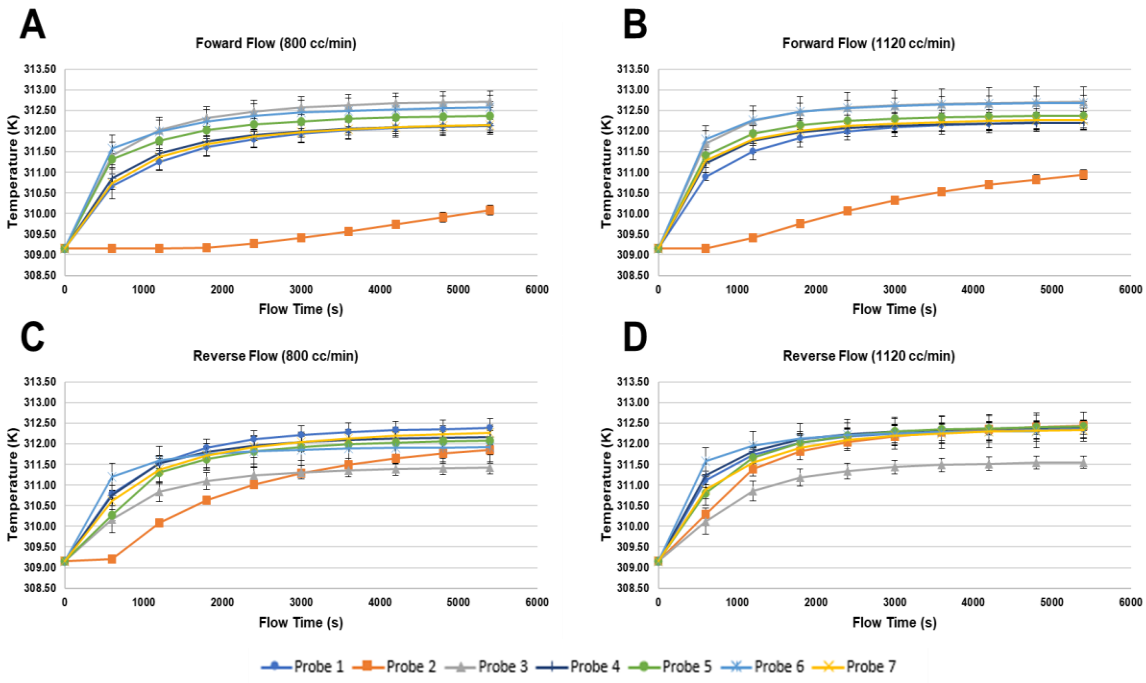

FIGURE 5 - Temperatures in the abdominal cavity at each probe location at 600s and 5400s of flow time. (A) Fluid temperature during forward (superior inlet) flow at 800cc/min flow; (B) Fluid temperature during forward (superior inlet) flow at 1120cc/min flow; (C) Fluid temperature during reverse (inferior inlet) flow at 800cc/min flow; (D) Fluid temperature during reverse (inferior inlet) flow at 1120cc/min flow; Error bars: SD, n=3.

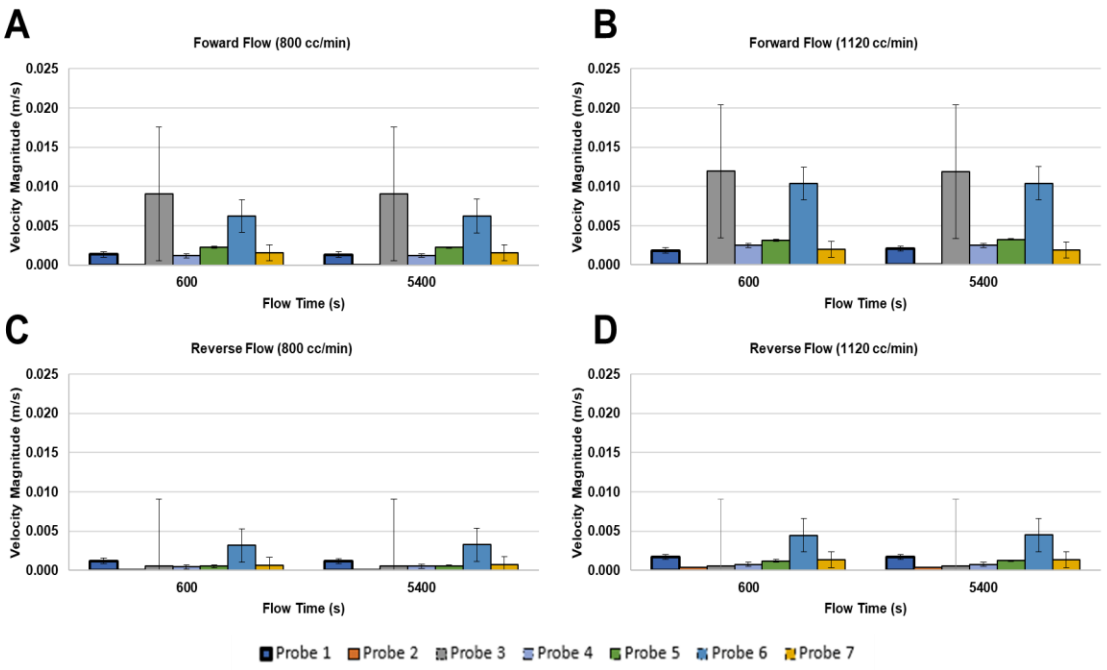

FIGURE 6 - Flow rates in the abdominal cavity at each probe location at 600s and 5400s of flow time. (A) Velocity magnitudes of flow during forward (superior inlet) flow at 800cc/min flow; (B) Velocity magnitudes of flow during forward flow (superior inlet) at 1120cc/min flow; (C) Velocity magnitudes of flow during reverse (inferior inlet) flow at 800cc/min flow; (D) Velocity magnitudes of flow during reverse flow (inferior inlet) flow at 1120cc/min flow. Error bars: SD, n=3.

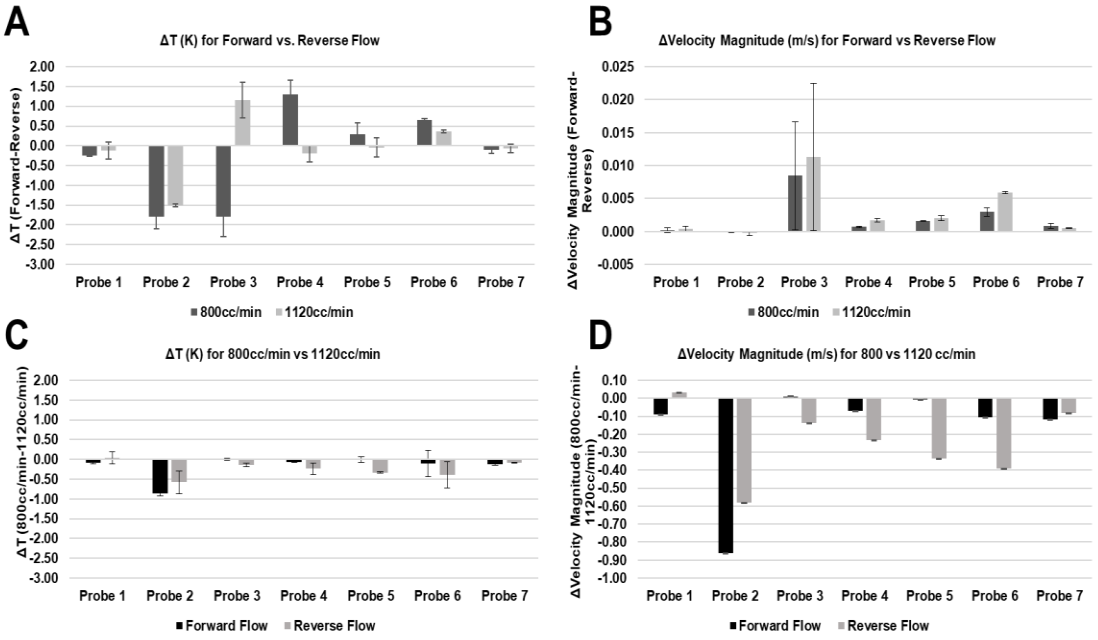

FIGURE 7 - Difference in fluid temperatures (ΔT) and in velocity magnitudes (ΔV) at each probe location at time 5400s. (A) Temperature difference between forward and reverse flow based on flow rate; (B) Difference in flow between forward and reverse flow based on flow rate; (C) Temperature difference between forward and reverse flow based on direction of flow; (D) Difference in flow between forward and reverse flow based on direction of flow. Error bars: SD, n=3. NOTE: Figure 7B has a different y-axis scale than Figure 7D.

CURRICULUM VITA

NAME:	Olivia Susan Cooney
ADDRESS:	Department of Bioengineering 220 Eastern Parkway University of Louisville Louisville, KY 40292
DOB:	January 9, 1999
EDUCATION & TRAINING	B.S., Bioengineering University of Louisville 2017-2021
	M.Eng., Bioengineering University of Louisville 2021-2023
AWARDS:	
PROFESSIONAL SOCIETIES:	
PUBLICATIONS:	
NATIONAL MEETING PRESENTATIONS:	
REFEREED JOURNALS:	

BOOKS AND SYMPOSIA:

INVITED PRESENTATIONS: